Non-parametric reconstruction of the galaxy-lens in PG1115+080

Prasenjit Saha
Department of Physics (Astrophysics)
Keble Road, Oxford OX1 3RH
saha@physics.ox.ac.uk

Liliya L.R. Williams
Institute of Astronomy
Madingley Road, Cambridge CB3 0HA
llrw@ast.cam.ac.uk

Abstract: We describe a new, non-parametric, method for reconstructing lensing mass distributions in multiple-image systems, and apply it to PG1115+080, for which time delays have recently been measured.

It turns out that the image positions and the ratio of time delays between different pairs of images constrain the mass distribution in a linear fashion. Since observational errors on image positions and time delay ratios are constantly improving, we use these data as a rigid constraint in our modelling. In addition, we require the projected mass distributions to be inversion-symmetric and to have inward-pointing density gradients. With these realistic yet non-restrictive conditions it is very easy to produce mass distributions that fit the data precisely.

We then present models, for $H_0 = 42$, 63 and 84 $\mathrm{km\,s^{-1}\,Mpc^{-1}}$, that in each case minimize mass-to-light variations while strictly obeying the lensing constraints. (Only a very rough light distribution is available at present.) All three values of H_0 are consistent with the lensing data, but require quite different morphologies for the lensing galaxy. If H_0 is low, the main lensing galaxy could be an early type. For intermediate H_0 the galaxy is reconstructed as a late elliptical or a highly inclined disc. High H_0 appears to require a nearly edge-on disc (or possibly a binary or merging system). Preliminary indications are that the galaxy is in fact an elliptical, which argues rather robustly against high H_0.

1. INTRODUCTION

The history of modeling of PG1115+080 is an illustrative example of how lens modeling has evolved in the last 15 years or so. The first published model of PG1115 (Young *et al.* 1981) considered a spiral galaxy-lens consisting of a highly flattened disk and a slightly flattened bulge. Since the two components had different velocity dispersions, scale lengths, and ellipticity, the model had 6 parameters even without the adjustable lens redshift. There were only six observational constraints. The acceptability of this over-specified yet realistic model went to show that the image configuration could easily arise from gravitational lensing. Later modelers demonstrated that the image configuration could be achieved with less parameters; Narasimha *et al.* (1983) used a single component lens: a truncated, mildly elliptical King profile. Kochanek (1991) fit five different models, each with 5 free parameters. With the arrival of more observational constraints, i.e. the galaxy position, more precise image positions (Kristian *et al.* 1993, hereafter K93, and Courbin *et al.* 1997), and time delays for the images (Schechter *et al.* 1997, hereafter S97), all the single galaxy parametric models became unacceptable (S97, Keeton & Kochanek 1997).[1]

A very plausible explanation is that nearby external galaxies contribute non-negligible shear, and possibly convergence at the location of the images. Adding external galaxies gives one at least two additional parameters, magnitude and position angle of the shear, and thus more freedom to fit the data. This approach has been explored by Witt & Mao (1997), and Keeton & Kochanek (1997). But as the observational constraints tighten should one use more elaborate parametric models with more free parameters to get acceptable fits to the observations? How far can one justify this approach?

Instead, we decided to explore the non-parametric models of galaxy mass distribution. In this paper we describe our modeling method and apply it to a quadruple gravitational lens system, PG1115+080. We show that the lensing observational constraints in this system (image positions and time delay ratio), combined with a few general, non-restrictive requirements for the galaxy mass distribution produce realistic galaxy models. In fact the plausible 'model-space' perfectly consistent with the lensing data is huge, much larger than current parametric models have explored.

2. OBSERVATIONS OF PG1115+080

PG1115+080 is a quadruply-lensed bright optical QSO, with well defined image positions (5 mas errorbars), a dominant lensing galaxy (50 mass position errorbars), and well constrained and easily observable time delays of $\sim$ several days to a couple of weeks. In this work we use image and galaxy positions as given by K93, based on HST data. The redshifts of the main lensing galaxy and other galaxies in the group are assumed to be $z = 0.311$ (Kundić *et al.* 1997). We use the time delays derived by BK97 based on the homogeneous photometric light curve data obtained by S97. BK97 estimates that B

[1] We have quoted the number of parameters in the various mass models; but there are also two extra parameters: the coordinates of the source. Authors disagree as to whether the source coordinates should count as extra parameters, and thus may reach different conclusions from a χ^2 test with the same models and data. Our own view, agreeing with S97, is that the source coordinates *should* be counted.

lags C by $25^{+3.3}_{-3.8}$ days, consistent with the S97's 23.7 ± 3.4 days. The delay between B and A is less certain, $\sim$10–14 days. The ratio between time delays consequently remains somewhat uncertain; BK97 estimates $t_{\rm AC}/t_{\rm BA} = 1.13^{+0.18}_{-0.17}$ compared with S97's $\simeq 0.6$.

We emphasize that not all observational constraints are equally good for the purposes of lens modeling, even if the observational errors are small. The best observables are the ones that depend on the global properties of the lens, with little sensitivity to local mass variations. For example, image fluxes are not reliable, while image positions are more stable. Time delays between images are also very good, but since time delays themselves involve H_0, we use the *ratio* of the two observed time delays, t_{AC}/t_{BA}. Thus we have 9 constraints: 8 from image positions, plus the time delay ratio. The observational errors on these quantities are already small, and are expected to keep on shrinking with more data. Therefore, we use these data as rigid constraints.

3. A LENS RECONSTRUCTION METHOD

Here we describe our method of non-parametrically reconstructing the galaxy mass distribution based on a observed lensing constraints, and a few general requirements for the galaxy. We take the lens as a pixellated mass distribution. It is simplest to leave masses in terms of the critical density, so we say that the nth pixel has surface density κ_n times

$$\Sigma_{\rm crit} = \frac{D_{\rm L} D_{\rm S}}{D_{\rm LS}} \frac{c^2}{4\pi G}, \tag{1}$$

$\Sigma_{\rm crit}$ being the critical surface mass density for lensing in units of mass per unit solid angle at the redshift of the lens. The nth pixel's contribution to the potential at some $\boldsymbol{\theta}$ is $\kappa_n \psi_n(\boldsymbol{\theta})$ and its contribution to the bending angle is $\kappa_n \boldsymbol{\alpha}_n(\boldsymbol{\theta})$, where

$$\begin{aligned} \psi_n(\boldsymbol{\theta}) &= \frac{1}{\pi} \int \ln|\boldsymbol{\theta} - \boldsymbol{\theta}'|\, d^2\boldsymbol{\theta}', \\ \boldsymbol{\alpha}_n(\boldsymbol{\theta}) &= \frac{1}{\pi} \int \frac{\boldsymbol{\theta} - \boldsymbol{\theta}'}{|\boldsymbol{\theta} - \boldsymbol{\theta}'|^2}\, d^2\boldsymbol{\theta}'. \end{aligned} \tag{2}$$

The integrals in (2) are over the n-th pixel, and depend on where $\boldsymbol{\theta}$ is relative to that pixel, and on the pixel size (say a). The integrals over square pixels for ψ_n and $\boldsymbol{\alpha}_n$ can be done exactly.

To get the full time delay and bending angle we sum over all pixels. For a source at $\boldsymbol{\theta}_{\rm S}$ the time delay is proportional to

$$\tau(\boldsymbol{\theta}) = \tfrac{1}{2}|\boldsymbol{\theta}|^2 - \boldsymbol{\theta} \cdot \boldsymbol{\theta}_{\rm S} - \sum_n \kappa_n \psi_n(\boldsymbol{\theta}). \tag{3}$$

(Compared to how (3) is usually written, we have dropped the term $\frac{1}{2}|\boldsymbol{\theta}_{\rm S}|^2$ because it cancels for all observable effects.) To get the time delay in physical units we have to multiply τ by

$$(1 + z_{\rm L}) \frac{D_{\rm L} D_{\rm S}}{c D_{\rm LS}}. \tag{4}$$

Images will appear where $\nabla\tau(\boldsymbol{\theta}) = 0$, or

$$\boldsymbol{\theta} - \boldsymbol{\theta}_{\mathrm{S}} - \sum_n \kappa_n \boldsymbol{\alpha}_n(\boldsymbol{\theta}) = 0. \tag{5}$$

Now, consider what lensing data imply when inserted into equations (3) and (5). First, the image positions in a multiple-image system tell us that $\nabla\tau(\boldsymbol{\theta}_i) = 0$ for some known $\boldsymbol{\theta}_i$. Each image provides two such constraint equations. From (5) we can see that these constraint equations are linear in the unknowns (κ_n and $\boldsymbol{\theta}_{\mathrm{S}}$). Secondly, if time delays have been measured between more than one pair of images, as in S97, then the ratio of time delays provides a constraint of the type

$$\tau(\boldsymbol{\theta}_4) - \tau(\boldsymbol{\theta}_1) = \langle \mathrm{ratio} \rangle \times (\tau(\boldsymbol{\theta}_2) - \tau(\boldsymbol{\theta}_1)). \tag{6}$$

Comparing with (3), we see that such constraints are also linear.

Thus the lensing data on PG1115+080 provide nine constraint equations, eight from the image positions and one from the time delay ratio. We will supplement these with some more constraints on physical grounds.

(i) Obviously, the κ_n must be non-negative.

(ii) The centroid of the lensing galaxy is known from K93, and we require the mass profile to be 180° rotation symmetric about this centroid. In other words $\kappa_{i,j} = \kappa_{-i,-j}$, where we are changing notation briefly from κ_n to $\kappa_{i,j}$ and $\kappa_{0,0}$ is centred on the galaxy centroid. We remark that without this constraint or some other that fixes the origin, the lensing data would have supplied only seven constraint equations.

(iii) For a galaxy we expect the density gradient to generally be pointing inwards. Accordingly, we define a pixellated density gradient

$$\nabla\kappa_{i,j} \equiv (2a)^{-1} \left(\kappa_{i+1,j} - \kappa_{i-1,j}\, ,\, \kappa_{i,j+1} - \kappa_{i,j-1}\right) \tag{7}$$

and require that $\nabla\kappa_{i,j}$ point no more than 45° away from radially inwards.

(iv) We require that $\tau(\mathrm{A1}) < \tau(\mathrm{A2})$, i.e., of the two A images, the southern one leads.[2]

(v) Though one can generate a mass profile and then calculate the implied H_0, in practice we found it more convenient to set H_0 at various values and generate different mass profiles at each value. Since the time scale (4) is $\propto H_0^{-1}$, fixing H_0 is just another linear constraint.

The foregoing are all linear equality and inequality constraints and it is straightforward to find, by linear programming, if there are any feasible mass distributions. If there are then there is not one mass model but a huge family of them, all consistent with the lensing data and our additional imposed constraints. At this point there are

---

[2] Given that C leads A leads B, there are two natural five-image configurations. One of them has A1, A2 and C as respectively minimum, saddle-point and mininum in a lemniscate, and B and the demagnified central image being respectively saddle-point and maximum in a limaçon. The other configuration has A1, A2 and C as respectively saddle-point maximum and mininum in a limaçon. (See Figure 6 in Blandford and Narayan 1986.) Both of these have A1 leading A2, and in fact we have only ever seen the former in models of the PG1115 system. Other configurations are logically possible, but would have contorted time delay surfaces.

several sensible things one can do. One might take some sort of average over all the allowed mass distributions. Or one might specify some figure of merit such as smoothness or entropy, and then optimize subject to all the above constraints. In this paper we will do the latter, choosing our optimal model as the one with minimum mass-to-light variation. More precisely, given a pixellated light distribution L_n for the galaxy, we find the mass distribution that minimizes

$$\sum_n (\kappa_n - KL_n)^2, \quad \text{where } K = \textstyle\sum_n \kappa_n, \ \sum L_n = 1, \tag{8}$$

subject to all the linear constraints above.

Our reconstruction procedure has a simple geometrical interpretation. Supposing there are N independent pixels, consider the N-dimensional space of the independent κ_n. The lensing constraints and H_0 specification confine allowed models to a $(N-8)$-dimensional hyperplane in this space. (There are ten equality constraints in all, but two of them go to solve for $\boldsymbol{\theta}_{\rm S}$.) The inequality constraints further confine allowed models to a convex region of the hyperplane. Now L_n is a point in the N-dimensional space, and a line from the origin through L_n represents constant mass-to-light models. Our optimal model is then the point on the allowed part of the $(N-8)$-hyperplane that is closest to that line.

The numerical problem has a unique solution, and quadratic programming algorithms reliably find it. We used the NAG routine E04NFF.

4. RECONSTRUCTIONS OF THE LENS

For the PG1115 system, the time scale factor (4) equals $31h^{-1}$ days arcsec^{-2} for $q_0 = \frac{1}{2}$. The q_0 dependence is weak. In the text we will write "$h = 0.5$" as shorthand for "$H_0 = 50$ km s^{-1} Mpc^{-1}for $q_0 = \frac{1}{2}$" and so on. The angular diameter distance of the lens is $D_{\rm L} = 2.77h^{-1}$ kpc arcsec^{-1} and the critical density $\Sigma_{\rm crit} = 3.30h^{-1} \times 10^{10} M_\odot$ arcsec^{-2}. The total mass in a pixellated reconstruction is

$$\Sigma_{\rm crit} \times a^2 \textstyle\sum_n \kappa_n. \tag{9}$$

We can define a formal Einstein radius $\theta_{\rm E}$ by equating $a^2 \sum_n \kappa_n$ to $\pi\theta_{\rm E}^2$. (It is only formal because the lensing mass isn't circular and doesn't produce Einstein rings.) Then the total mass is

$$\theta_{\rm E}^2 \times 1.04 \times 10^{11} h^{-1} M_\odot \ \text{arcsec}^{-2}. \tag{10}$$

We can use equation (10) to associate formal Einstein rings with the other group galaxies too; it's a convenient way to show various masses on a figure.

In this section, we illustrate three reconstructions in detail. All have $0.1''$ mass pixels and confine the main lensing galaxy to a circle of radius $2''$ around the centroid measured by K93. The other group galaxies are considered as three point masses. We did not find our reconstructions sensitive to the pixel size and maximum galaxy radius. For the light distribution against which we optimize we used the K93 model

$$L(\boldsymbol{\theta}) = \left(1 + \frac{|\boldsymbol{\theta}|^2}{\theta_0^2}\right)^{-\gamma/2}, \quad \theta_0 = 0.71'', \ \gamma = 1.7. \tag{11}$$

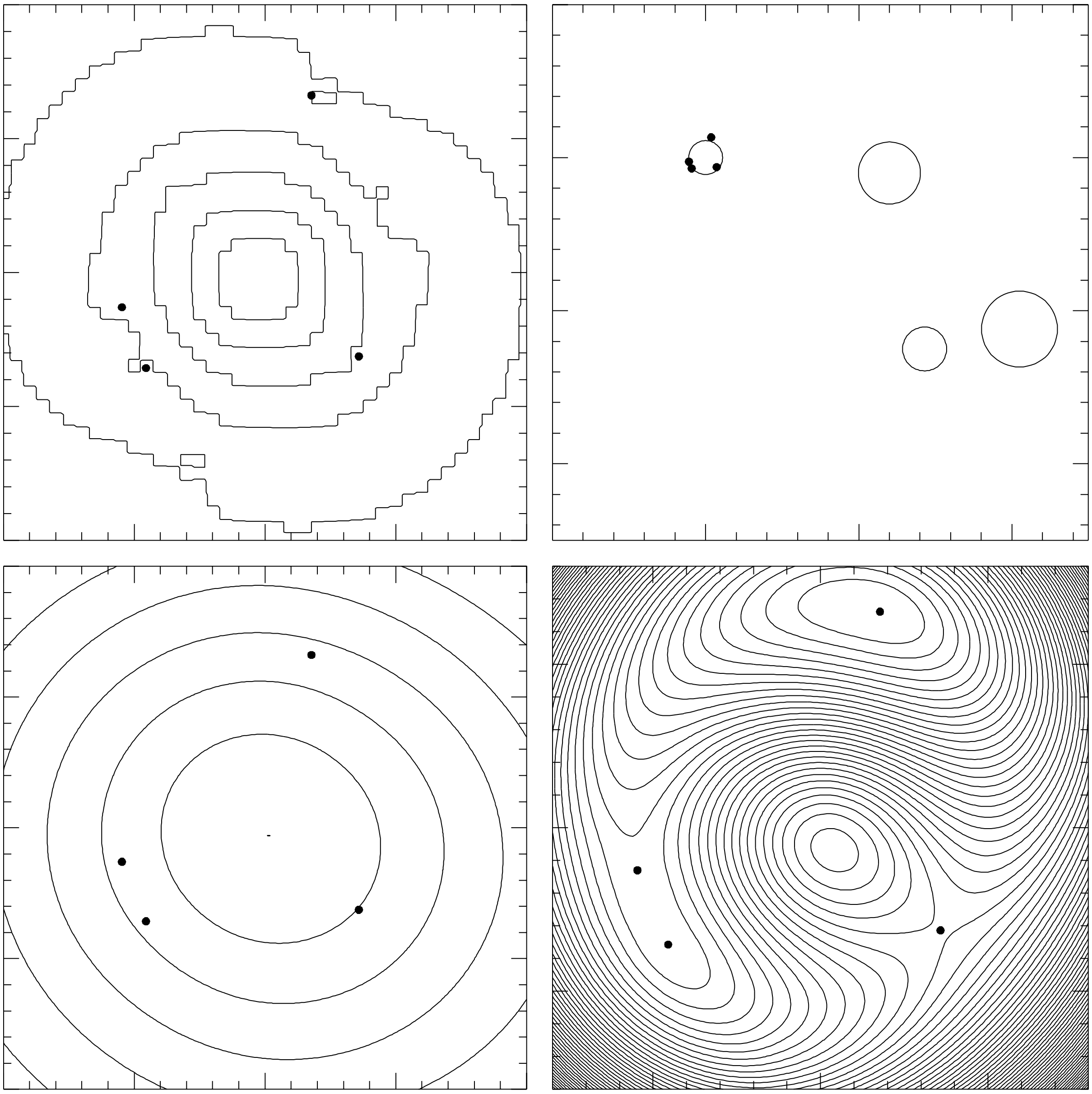

Figure 1. A reconstruction constrained by the image positions from K93 and the time delays from BK97's re-analysis of S97, and by $h = 0.42$. We have suppressed axis labels to reduce clutter, but the image positions (marked by filled circles) in each panel should make the scales clear.

Upper left panel: Contours of the dimensionless surface density $\kappa = \frac{1}{3}, \frac{2}{3}, \ldots$, increasing inwards. The field shown is $(-2'', -2'')$ to $(2'', 2'')$ with the galaxy centroid from K93 at the origin.

Lower left panel: Contours of $\boldsymbol{\theta} \cdot \boldsymbol{\theta}_{\rm S} + \psi(\boldsymbol{\theta})$, increasing outwards in steps of $\frac{1}{2}$ arcsec^2. The field is as in the upper panel.

Lower right panel: Time delay contours, in steps of 1 day. The field shown is $(-1.6'', -1.6'')$ to $(1.6'', 1.6'')$ with the same origin.

Upper right panel: The field shown here is $(-10'', 25'')$ to $(-25'', 10'')$ relative to the same origin as before. The galaxy masses are indicated by formal Einstein rings (see equation 10).

Again, our reconstructions are not at all sensitive to this. On the basis of the magnitudes in K93 we loosely constrained the allowed mass range of these galaxies (usually known as G1, G2, G3) relative to the main lensing galaxy G as follows: (i) The total mass of

G1, G2 and G3 is no more than 10 times that of G; (ii) each of G1, G2 and G3 has more mass than G; (iii) G1 has more mass than G2 and G3 put together; (iv) G2 and G3 are at most a factor of 2 apart in mass. The masses of the galaxies, one of the outputs of the code, are proportional to the area of the circle in the diagrams.

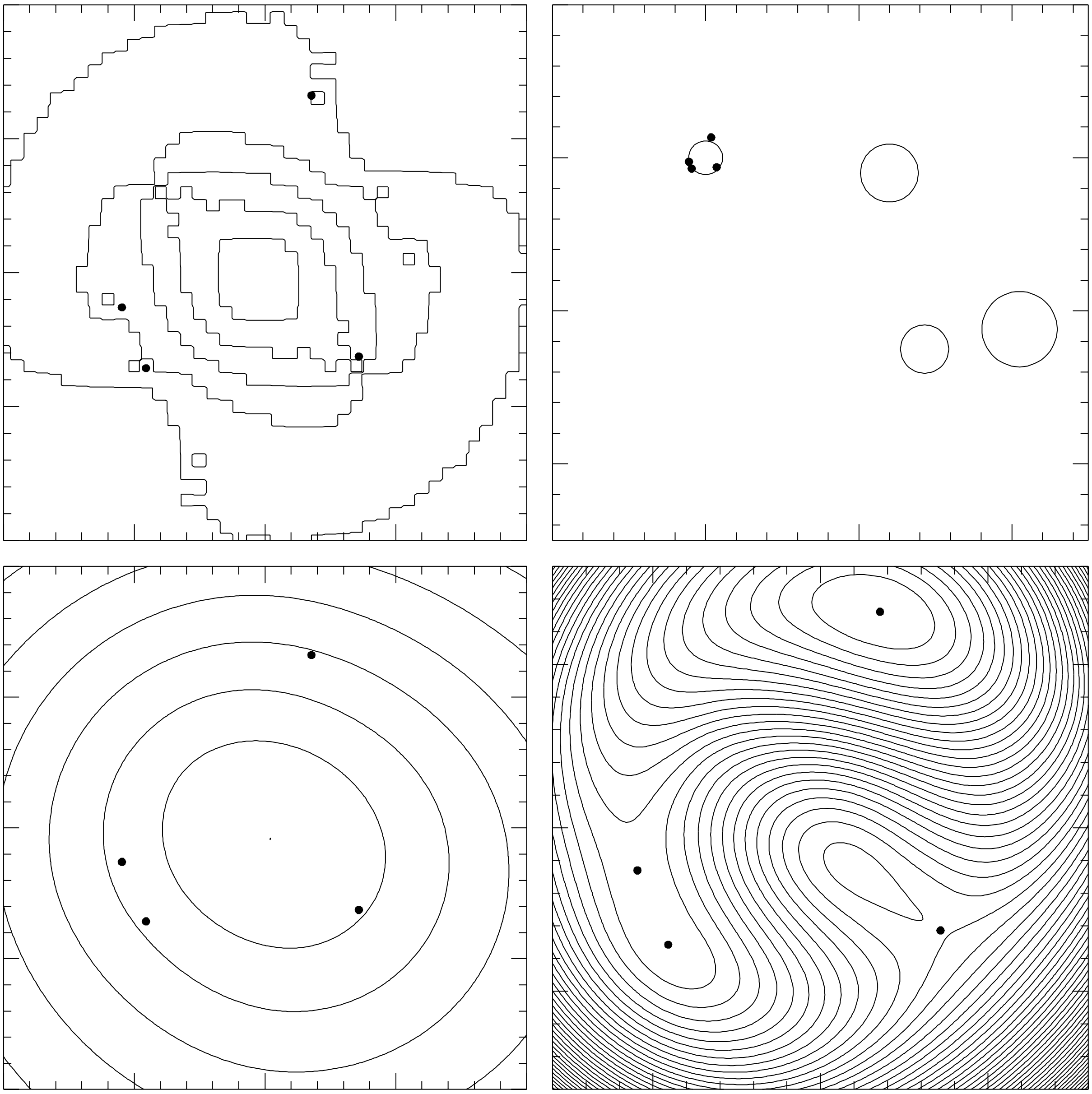

Figure 2. Like Figure 1, except that $h = 0.63$.

As we already pointed out, realistic galaxy profiles are easy to obtain with our method, hence h is not usefully constrained by the current observations in this lens system. Since this is the case, we decided to carry out mass reconstructions for three plausible values of h. Figure 1 is constrained by $h = 0.42$, Figure 2 by $h = 0.63$ and Figure 3 by $h = 0.84$. We chose these values to coincide with the range found by S97 in their modelling.

Density map: The 180° rotation symmetry allows isodensity contours to twist, and this seems to be generic feature of our reconstructions though it is not always as pronounced as in this model. Some parametric models get a similar effect by using

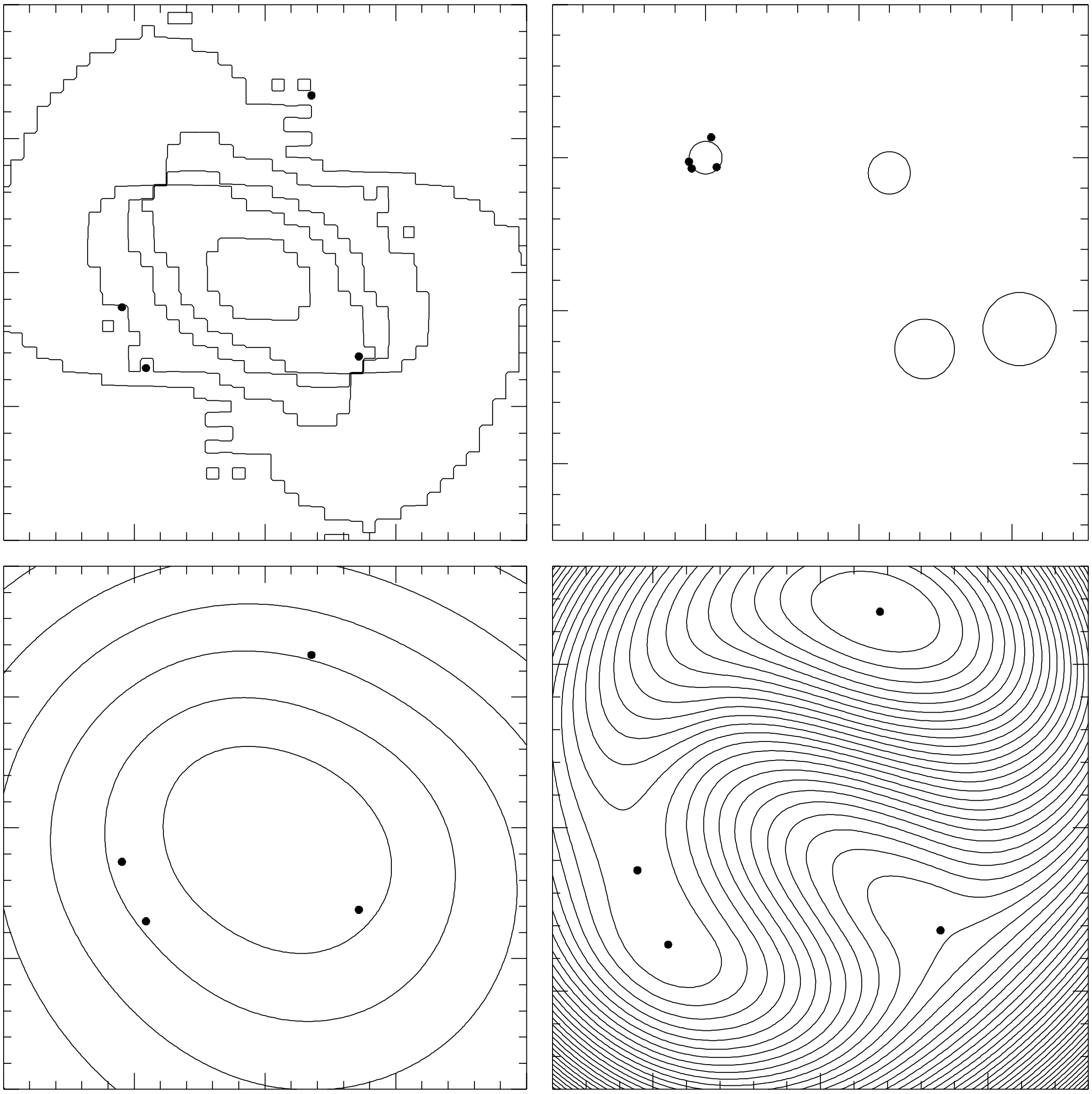

Figure 3. Like Figures 1 and 2, except now $h = 0.84$.

two shear axes. (Incidentally, the single-pixel peaks in the density map may seem inconsistent with our density gradient constraint. But because $\nabla\kappa_{ij}$ is formulated as a symmetric difference in equation 7, such single-pixel blemishes are in fact tolerated by the constraint.)

Lens potential: We plot $\boldsymbol{\theta}_{\rm S} \cdot \boldsymbol{\theta} + \psi(\boldsymbol{\theta})$ rather than $\psi(\boldsymbol{\theta})$ itself. Comparing with models that include the external galaxies, we have found that both $\boldsymbol{\theta}_{\rm S}$ and $\psi(\boldsymbol{\theta})$ change drastically on including those galaxies, but $\boldsymbol{\theta}_{\rm S} \cdot \boldsymbol{\theta} + \psi(\boldsymbol{\theta})$ (like the time delay surface) changes very little. In a sense there is a degeneracy between $\boldsymbol{\theta}_{\rm S}$ and the mass distribution, and in the plot we have used it to nominally move the source to the origin. It is remarkable how much smoother the potential is than the density; of course the smoothness comes from having integrated the density twice with a $\ln|\boldsymbol{\theta} - \boldsymbol{\theta}'|$ kernel.

Time delay contours: We have spaced the contours by 1 day, and this plot provides a pleasing visual check that our fitting program does what it is supposed to do.

From this plot the central image may seem worryingly bright, but this is not really an issue. The reconstructions in this paper all have wide cores simply because the simple K93 light model does. But we could imagine reshaping the core in a circularly symmetric way to have a central density cusp; this would demagnify the central image without affecting the positions or time delays of the other images.

The mass distribution looks different in the three cases. For $h = 0.42$, the galaxy is reconstructed as a possible early-type, or a face-on spiral. For $h = 0.84$, the galaxy is rather elongated, and so could be an edge-on disc, or highly flattened elliptical. Note that in all three cases, the major axis is aligned with the major axis of the group. The effect is barely noticeable for a low Hubble constant (see outer isophotes in Figure 1), and is most pronounced for a high Hubble constant. Is this alignment physically motivated? No convincing observational data exists for or against the alignment of galaxies in groups; however numerical simulations may indicate that such alignment is possible (Ciotti & Dutta 1994).

Figures 1–3 indicate that higher values of h require more elliptical mass distribution in the lensing galaxy. This can be intuitively understood as follows. The time delay between any two images, $[(1+z_{\rm L})D_{\rm L}D_{\rm S}/cD_{\rm LS}]\cdot[\tau(\boldsymbol{\theta}_1)-\tau(\boldsymbol{\theta}_2)]$, where $\tau(\boldsymbol{\theta})$ is given by equation (3), is inversely proportional to h. Since time delays are fixed by observations, a higher value of h necessitates the scaled time delays, $\tau(\boldsymbol{\theta}_1)-\tau(\boldsymbol{\theta}_2)$ to be proportionately larger. The scaled time delays between roughly equally spaced (quadruple) images tend to be larger for elliptical lenses: The time delay surface consists of a geometrical and gravitational part (see equation [3]), that are added together. The images are formed at stationary points of the resulting surface, and the time delay between them is just the difference in the 'height' of the time delay surface at the image points. Then one can see that in general, when the gravitational potential of an elliptical lens is added to the geometrical part, the resulting stationary points will lie at more varied heights, implying larger scaled time delays, compared to a case with a circularly symmetric lens. Therefore, more elliptical lenses require larger h, if the observed time delays are fixed.

We have made reconstructions using image positions from Courbin et al. (1997), but these differ only very slightly from the ones presented here. We have also tried making models without the external galaxies—that works too, with the necessary shear being supplied by a twisting galaxy density.

5. CONCLUSIONS

In a multiple-image QSO, the time delay between two images can be written as

$$H_0^{-1}D(z,q_0)F_{\rm lens}$$

where $D(z,q_0)$ is a dimensionless factor depending on the source and lens redshifts and (weakly) on q_0, and $F_{\rm lens}$ is of order the image separation but its exact value depends on the distribution of the lensing mass. The uncertainty in H_0 estimates from lensing comes almost entirely from the uncertainty in $F_{\rm lens}$. The recent measurement by S97 of time delays in PG1115+080 are an important advance, because positions of four images, rather than two, and time delay measurements between two pairs of images, rather than one pair, provide help constrain $F_{\rm lens}$ much better than in two-image systems, like Q0957+561 A&B.

We have developed a non-parametric or free-form lens modelling technique to explore the consequences of these excellent new data. It turns out that image positions and time delay ratios constrain a pixellated mass distribution through linear equations. Assumptions like 180° rotation symmetry and density gradient always pointing inwards are also readily cast as linear constraints. Implementing all this, we find that it is almost embarrassingly easy to fit the lensing data for any plausible H_0 with plausible looking models.

We then try to pose a somewhat different question: what do different ranges of H_0 imply about the lensing galaxy that might possibly be distinguished by detailed observations of it? (As present only a centroid and a circular model for the galaxy light profile are available.) Some indications might be given by examining mass models that, while satisfying the lensing data, follow the light as closely as possible. We construct such models for $h = 0.42$, 0.63 and 0.84. The $h = 0.42$ model has a mildly elliptical mass profile with some twist in the isodensity contours. The $h = 0.63$ model has significant ellipticity inwards of the images; such a system could be a late elliptical, but a very inclined disc would be more likely. For $h = 0.84$ the ellipticity needed is still more, perhaps too much to be an elliptical. It is also curious that the ellipticity is aligned with the group direction.

In other words, our reconstructions imply different conclusions for H_0 depending on the morphology of the galaxy. Now the mass interior to the images ($\sim 10^{11}h^{-1}M_\odot$ within $\sim 3h^{-1}$kpc) the colour, the spectrum of the galaxy (Kundić *et al.* 1997), and its velocity dispersion, 280-290 km.s^{-1} (Tonry 1997) are all indicative of an elliptical. This argues strongly against high H_0. But further conclusions must await more data on the morphology.

REFERENCES

Bar-Kana, R. 1997, Preprint, also available as astro-ph/9701068 (BK97)

Blandford, R., & Narayan, R. 1986, ApJ, 310, 568

Courbin, F., Magain, P., Keeton, C. R., Kochanek, C. S., Vanderriest, C., Jaunsen, A. O. & Hjorth, J. 1997, Preprint, also available as astro-ph/9705093

Keeton, C. R., & Kochanek, C. S. 1997, Preprint, also available as astro-ph/9611216

Kochanek, C. S. 1991, ApJ, 373, 354

Kristian, J. *et al.* 1993, AJ, 106, 1330 (K93)

Kundić, T., Cohen, J. G., Blandford, R., D., & Lubin, L. M. 1997, Preprint, also available as astro-ph/9704109

Narasimha, D., Subramanian, K., & Chitre, S. M. 1982, MNRAS, 200, 941

Schechter, P. L., *et al.* 1997, ApJL, 475, L85 (S97)

Tonry, J. L. 1997, Preprint, also available as astro-ph/9706199

Witt, H.-J., & Mao, S. 1997, Preprint, also available as astro-ph/9702021

Young, P., Deverill, R. S., Gunn, J. E., Westphal, J. A., & Kristian, J. 1981, ApJ, 244, 723